

Towards a general parametrization of the warm dark matter halo mass function

MARK R. LOVELL¹

¹*University of Iceland
Dunhaga 5
107 Reykjavík, Iceland*

(Received February ..., 2020; Revised February ..., 2020; Accepted February ..., 2020)

Submitted to ApJ

ABSTRACT

Studies of flux anomalies statistics and perturbations in stellar streams have the potential to constrain models of warm dark matter (WDM), including sterile neutrinos. Producing these constraints requires a parametrization of the WDM mass function relative to that of the cold dark matter (CDM) equivalent. We use five WDM models with half-mode masses, $M_{\text{hm}} = [1.3, 35] \times 10^8 M_{\odot}$, spread across simulations of the Local Group, lensing ellipticals and the $z = 2$ universe, to generate such a parametrization: we fit parameters to the functional form $n_{\text{WDM}}/n_{\text{CDM}} = (1 + (\alpha M_{\text{hm}}/M_X)^{\beta})^{\gamma}$. For $M_X \equiv$ virial mass of central halos we obtain $\alpha = 2.3$, $\beta = 0.8$, and $\gamma = -1.0$, and this fit is steeper than the EPS formalism predicts. For $M_X \equiv$ mass of subhalos we instead obtain $\alpha = 4.2$, $\beta = 2.5$ and $\gamma = -0.2$; in both mass definitions the scatter is ~ 20 per cent. However, we caution that robust constraints will require bespoke simulations and a careful definition of halo mass, particularly for subhalos of mass $< 10^8 M_{\odot}$.

Keywords: dark matter:warm dark matter

1. INTRODUCTION

Recent observations of various astrophysical observables have opened up the possibility of measuring the dark matter halo mass function at redshifts $z < 0.5$. Lensing flux-anomalies studies (Hsueh et al. 2019; Gilman et al. 2019) and an analysis of gaps in stellar streams around the Milky Way (MW) (Banik et al. 2019) have claimed to detect large numbers of dark matter halos at the mass scale of $10^8 - 10^9 M_{\odot}$. These analyses then offer the opportunity to place constraints on the presence, or otherwise, of a cut-off in the linear matter power spectrum, which can then provide information about whether the dark matter particle belongs to the cold dark matter (CDM) family of candidates – WIMPs, QCD axions – if there is an absence of a cut-off at wavenumbers $k < 100 h/\text{Mpc}$, or instead to the warm dark matter (WDM) family, such as sterile neutrinos.

The crucial step for comparing observational results to dark matter models is an accurate prediction for the

halo mass function in each model. Parametrizing the CDM halo mass function is now a well established practice. In its simplest form it is set by the cosmological parameters (e.g. Ludlow et al. 2016), although baryon physics introduces very significant uncertainty. The WDM case has proved much more challenging, for two reasons. First, WDM differs from CDM in that it constitutes a set of cosmologically distinct models, and the rich phenomenology of the sterile neutrino power spectra exhibits a wide variety of cut-off shapes and slopes (Lovell et al. 2016). Second, WDM simulations suffer from the spurious fragmentation of filaments, which generates many more halos than the physical model would predict (Wang & White 2007) and therefore measures have to be taken to avoid overestimating the halo abundance.

The standard approach to this problem of parametrizing the WDM halo mass function has been to multiply the CDM mass function by a WDM fitting function, R_{fit} , as derived from comparing CDM and WDM simulations of the same volume, i.e.: $R_{\text{fit}} = n_{\text{WDM}}/n_{\text{CDM}}$, where n_{WDM} and n_{CDM} are the differential halo mass functions of the WDM and CDM simulations respec-

tively. These include the fit to halos in a cosmological box by [Schneider et al. \(2012\)](#), and the fit to subhalos of a MW-analog halo reported by [Lovell et al. \(2014\)](#). Both of these early studies had drawbacks: [Schneider et al. \(2012\)](#) did not consider subhalos; [Lovell et al. \(2014\)](#) instead used a zoomed simulation of just one MW-analog halo such that it is not clear whether the results could be generalized across many halos, and both studies used WDM models warmer than are typically accepted as viable today. [Lovell \(2020\)](#) argued that such fits offer a poor approximation to extended Press-Schechter (EPS [Press & Schechter 1974](#); [Benson et al. 2013](#)) expectations for the mass function. Both fits used variations on the [Bode et al. \(2001\)](#) and [Viel et al. \(2005\)](#) thermal relic power spectra, which have different shapes to the particle physics-motivated sterile neutrino power spectra.

The best method currently available for making such comparisons to observations is to specify the dark matter model parameters and observable of interest, and then perform N -body/hydrodynamical simulations of this system. This approach was taken for lensing arc analyses by [Despali et al. \(2020\)](#), who used simulations of lensing halos at $z = 0.2$ that featured two distinct sterile neutrino models plus the [Lovell et al. \(2014\)](#) algorithm for removing spurious subhalos. Running high resolution simulations of this sort is computationally expensive, thus it is the exception rather than the rule.

In this *Letter* we instead use a wide variety of simulations of different environments and sterile neutrino models to derive approximations for R_{fit} , with separate R_{fit} for centrals/isolated halos on the one hand and for subhalos on the other. The purpose of these fits is to provide a first order understanding of whether a given model is in tension with the observational data: we reiterate that the ability to reject any model with certainty requires bespoke simulations of the sort run by [Despali et al. \(2020\)](#).

This *Letter* is organised as follows. In [Section 2](#) we present the simulations and our derived halo mass functions, and in [Section 3](#) we draw our conclusions.

2. SIMULATIONS AND RESULTS

The simulations used in this paper are derived from three simulation suites. We use the APOSTLE (AP) WDM simulations presented in [Lovell et al. \(2017\)](#), [Lovell et al. \(2019\)](#) and [Lovell et al. \(in prep.\)](#); the lensing halo (LH) simulations of [Despali et al. \(2020\)](#), and a previously unpublished simulation of a WDM 25 Mpc uniform resolution, cosmological box (L25) that was run to $z = 2$. These simulations were derived from CDM counterparts: the AP simulations in [Fattahi et al. \(2016\)](#)

and [Sawala et al. \(2016\)](#), the LH simulations from [Oppenheimer et al. \(2016\)](#) and the L25 from [Schaye et al. \(2015\)](#). All of the simulations were run with a variation of the EAGLE galaxy formation code ([Schaye et al. 2015](#)); AP was performed with the EAGLE REFERENCE (‘Ref’) model parameters, and LH and L25 with the RECALIBRATED (‘Rec’) parameters.

The halos were identified with the friends-of-friends (FoF) algorithm and decomposed into subhalos using the SUBFIND code ([Springel et al. 2001](#); [Dolag et al. 2009](#)). The largest SUBFIND halo in each FoF halo is defined as the central halo, and all other SUBFIND halos as subhalos / satellites. Spurious subhalos were flagged and removed with the Lagrangian region sphericity method of [Lovell et al. \(2014\)](#), using a sphericity cut $s = 0.2$; note that we do not also apply their cut on halo mass. The AP simulations were performed with the WMAP7 cosmological parameters ([Komatsu et al. 2011](#)) whereas the other simulations instead used parameters derived from the first Planck results ([Planck Collaboration et al. 2014](#)). The AP (LH) simulations are zoomed simulations, and therefore we only use halos/subhalos that are < 3 pMpc (< 4 pMpc) from the system centre-of-potential, whereas for the L25 simulations we use halos from the entire box.

We use five sterile neutrino models. Each model is described by two parameters: a sterile neutrino mass and a lepton asymmetry, L_6 ; see [Lovell et al. \(2016\)](#) for a discussion of these quantities. All five models use a sterile neutrino mass of 7 keV. The L_6 applied, from order of most extreme (‘warmest’) to most like CDM, are: $L_6 = 120$ (labeled LA120), the warmest of any 7 keV sterile neutrino; $L_6 = 11.2$ (LA11), the warmest consistent with the sterile neutrino dark matter decay interpretation of the unexplained 3.55 keV X-ray line ([Boyarisky et al. 2014](#); [Bulbul et al. 2014](#)); $L_6 = 10$ (LA10), an intermediate case; $L_6 = 9$ (LA9), the coldest consistent with the 3.55 keV line; and finally $L_6 = 8$ (LA8) which the coldest of any 7 keV sterile neutrino. The matter power spectra of these five models are shown in [fig. 1 of Lovell et al. \(2017\)](#).

The LA120 model was applied in six medium resolution (MR) AP volumes and the L25 box; LA11 in one high resolution (HR) AP volume and four LH volumes; LA10 in six MR AP simulations; LA9 in a single HR AP volume and LA8 in four LH simulations. The important properties of all the simulations used in this letter are included in [Table 1](#).

The goal of our analysis is to derive a set of fitting functions to the mass function, R_{fit} . We adopt the following function:

Table 1. Table of simulations used in this study. The columns are: simulation set name, number of volumes used in each set, type of dark matter model, parent simulation suite, galaxy formation model, mass of the simulation dark matter particle, final redshift of the simulation, cosmology from which the cosmological parameters were derived, half-mode mass of the dark matter model, and the references to the original papers, which are: (1) Lovell et al. (2019), (2) Lovell et al. in prep., (3) Lovell et al. (2017), (4) Sawala et al. (2016), (5) Despali et al. (2020) (6) Oppenheimer et al. (2016) and (7) Schaye et al. (2015).

Simulation	N_{vols}	DM model	GF model	Suite	$m_{\text{DM}} [M_{\odot}]$	z	Cosmology	$M_{\text{hm}} [M_{\odot}]$	Original paper
AP-LA11	1	LA11	Ref	AP-HR	5×10^4	0	WMAP7	9.2×10^8	(1)
AP-LA9	1	LA9	Ref	AP-HR	5×10^4	0	WMAP7	2.6×10^8	(2)
AP-LA120	6	LA120	Ref	AP-MR	6×10^5	0	WMAP7	3.1×10^9	(3)
AP-LA10	6	LA10	Ref	AP-MR	6×10^5	0	WMAP7	5.3×10^8	(3)
AP-CDM(HR)	1	CDM	Ref	AP-HR	5×10^4	0	WMAP7	N/A	(4)
AP-CDM(MR)	6	CDM	Ref	AP-MR	6×10^5	0	WMAP7	N/A	(4)
LH-LA11	4	LA11	Rec	Lens Halo	2×10^6	0.2	Planck	9.4×10^8	(5)
LH-LA8	4	LA8	Rec	Lens Halo	2×10^6	0.2	Planck	1.3×10^8	(5)
LH-CDM	4	CDM	Rec	Lens Halo	2×10^6	0.2	Planck	N/A	(6)
L25-LA120	1	LA120	Rec	25 Mpc box	1×10^6	2	Planck	3.5×10^9	This work
L25-CDM	1	CDM	Rec	25 Mpc box	1×10^6	2	Planck	N/A	(7)

$$R_{\text{fit}} = n_{\text{WDM}}/n_{\text{CDM}} = (1 + (\alpha M_{\text{hm}}/M_{\text{x}})^{\beta})^{\gamma}, \quad (1)$$

where M_{x} is the halo mass, for a given halo mass definition, and α , β and γ are three fitting parameters. M_{hm} is the half-mode mass, which is defined as the mass scale that corresponds to the power spectrum wavenumber at which the square root of the ratio of the WDM and CDM power spectra is 0.5. The value of M_{hm} for each simulation is given in Table 1: note that because M_{hm} is sensitive to the cosmological parameters, it can vary by a few per cent between simulations with the same DM model.

We adopt two definitions of halo mass. For central halos we use the virial mass, M_{200} , defined as the mass enclosed within the radius of overdensity 200 times the critical density required for collapse. For subhalos we instead use the gravitational bound mass as determined by SUBFIND, M_{SUBs} . We obtain separate fits – i.e. separate sets of α , β and γ values – for the two mass definitions. We start with M_{200} , plotting the ratios of n_{WDM} and n_{CDM} as a function of M_{200} in Fig. 1.

We obtain a fit that diverges by less than 50 per cent in all of the mass bins $> 10^8 M_{\odot}$ that contain more than ten haloes. In lower mass bins, resolution effects in both WDM and CDM simulations are expressed. The parameters of this fit are: $\alpha = 2.3$, $\beta = 0.8$, and $\gamma = -1.0$, for an asymptotic low mass slope of -0.8 . Our fit works particularly well for the LA8 and LA9 models, producing agreement better than 20 per cent, whereas LA120 is more challenging. There is a systematic bias for the fit to underestimate the number of LA120 halos at $\sim 10^9 M_{\odot}$ and overestimate it at $\sim 10^8 M_{\odot}$. This suggests that LA120 prefers a steeper fit than the other models, which

may reflect the fact that the LA120 linear matter power spectrum cut-off is steeper than those of the other models. These fits are somewhat steeper than the EPS mass functions calculated by Lovell (2020). There are no conspicuous variations between fits attained in different environments, e.g. Local Groups vs. lensing halos. We repeat this exercise for the SUBFIND bound mass of satellite halos, M_{SUBs} , in Fig. 2.

The parameters obtained for the satellite M_{SUBs} are $\alpha = 4.2$, $\beta = 2.5$ and $\gamma = -0.2$: the asymptotic slope is -0.5 and therefore shallower than for M_{200} ; also, the turnover occurs at lower masses. This picture is consistent with the observation in Bose et al. (2016) that the difference between CDM and WDM increases for later forming halos, given that centrals form later than satellites. Another example of this is comparing the $z = 2$ L25 simulation to the AP-LA120 volumes, where the former shows an excess of $10^7 M_{\odot}$ halos over the latter. In several instances the fit overestimates the abundance of $M_{\text{SUBs}} < 10^8 M_{\odot}$ halos by ~ 20 per cent, except for LA8 where instead it is $2 \times 10^9 M_{\odot}$ halos that are underestimated. We stress that this result relies on a particular definition of subhalo mass, and alternative subhalo finders may return very different results (Onions et al. 2012).

3. CONCLUSIONS

In this study we revisited the issue of parametrizing the suppression of the halo mass function in warm dark matter (WDM) relative to cold dark matter (CDM), taking advantage of hydrodynamical simulations at a variety of redshifts – $z = 0, 0.2$ and 2 – and regimes – the Local Group, lensing ellipticals and a uniform cosmological box – to produce a fit for the purposes of first

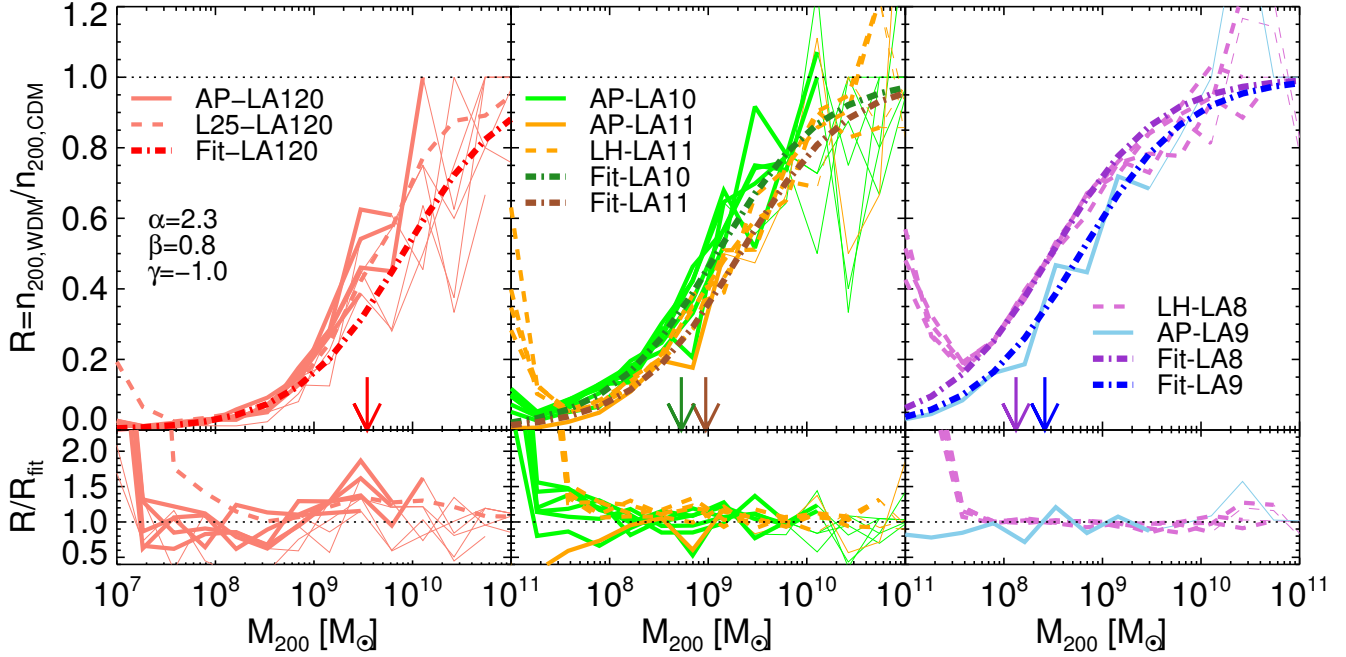


Figure 1. Ratio of WDM to CDM mass functions for central halos using the M_{200} definition of mass. Top panels: the ratio of the WDM mass function to its CDM counterpart for models LA120 (red curves, left-hand panel), LA10 and LA11 (green and orange curves respectively, middle panel), and LA8 and LA9 (purple and blue curves respectively, right-hand panel). In all three panels, the solid curves indicate AP volumes. The dashed curves indicate the L25 box in the left-hand panel and the LH volumes in the other two panels. The fits are shown as dot-dashed curves, with a color darker than the corresponding model: the parameters of the fit are displayed in the left-hand panel. Bottom panels: the ratio of the data curves to the fit. In both sets of panels, curves are drawn thin where each mass bin contains fewer than ten WDM halos and are drawn thick elsewhere. The arrows mark M_{hm} for each of the models: where we use results from both Planck and WMAP7-derived simulations (LA120 and LA11) we plot the arrow using the Planck M_{hm} only.

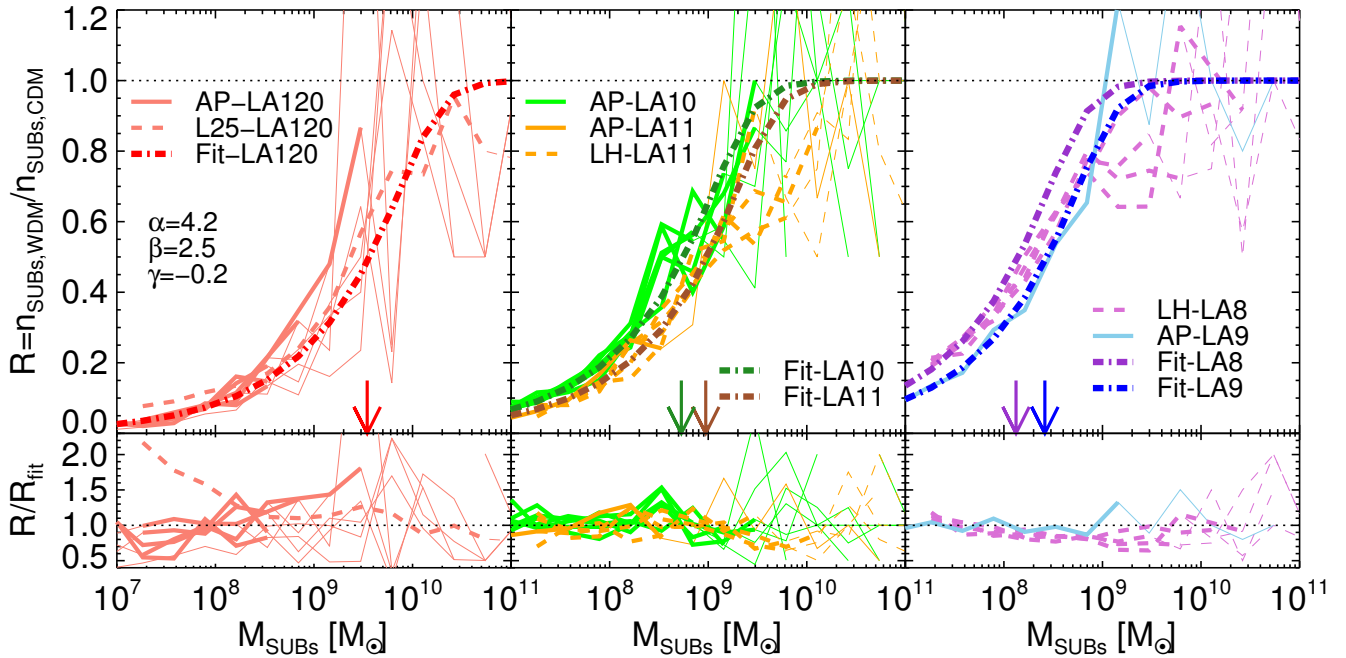


Figure 2. As for Fig. 1, but for subhalos using the SUBFIND bound mass, M_{SUBS} .

order comparisons between WDM models and observations. We find that the central halo, M_{200} differential mass function is approximated to typically better than 20 per cent using equation 1 with parameters $\alpha = 2.3$, $\beta = 0.8$, and $\gamma = -1.0$. Performing a fit on the subhalo, M_{SUBs} differential mass function, with the same functional form, we obtain $\alpha = 4.2$, $\beta = 2.5$ and $\gamma = -0.2$, although the accuracy of this subhalo fit to the simulations is not as consistent as the M_{200} fit.

These fits are to be understood as first order approximation of each mass function. The simulations assume a particular model of galaxy formation and alternative implementations of feedback could return different results. Fitting the subhalo results is particularly challenging; future studies that invoke general fits such as those presented here will ultimately need to be backed up by bespoke, observables-oriented simulations, will need a clear definition of halo mass, and must take account of the differences between halo finders in order to claim definitive constraints on a given dark matter model.

ACKNOWLEDGMENTS

MRL is grateful to the owners of the CDM simulations for their willingness to share their data, and would like to thank Wojtek Hellwing and Jesús Zavala for useful comments on the text. MRL acknowledges support by a Grant of Excellence from the Icelandic Research Fund (grant number 173929). This work used the DiRAC@Durham facility managed by the Institute for Computational Cosmology on behalf of the STFC DiRAC HPC Facility (www.dirac.ac.uk). The equipment was funded by BEIS capital funding via STFC capital grants ST/K00042X/1, ST/P002293/1, ST/R002371/1 and ST/S002502/1, Durham University and STFC operations grant ST/R000832/1. DiRAC is part of the National e-Infrastructure. Part of this work was carried out on the Dutch National e-Infrastructure with the support of SURF Cooperative. This project has also benefited from numerical computations performed at the Interdisciplinary Centre for Mathematical and Computational Modelling (ICM) University of Warsaw under grants #no GA67-15, GA67-16 and G63-3

REFERENCES

- Banik, N., Bovy, J., Bertone, G., Erkal, D., & de Boer, T. J. L. 2019, arXiv e-prints, arXiv:1911.02663
- Benson, A. J., Farahi, A., Cole, S., et al. 2013, MNRAS, 428, 1774
- Bode, P., Ostriker, J. P., & Turok, N. 2001, ApJ, 556, 93
- Bose, S., Hellwing, W. A., Frenk, C. S., et al. 2016, MNRAS, 455, 318
- Boyarsky, A., Ruchayskiy, O., Iakubovskyi, D., & Franse, J. 2014, Physical Review Letters, 113, 251301
- Bulbul, E., Markevitch, M., Foster, A., et al. 2014, ApJ, 789, 13
- Despali, G., Lovell, M., Vegetti, S., Crain, R. A., & Oppenheimer, B. D. 2020, MNRAS, 491, 1295
- Dolag, K., Borgani, S., Murante, G., & Springel, V. 2009, MNRAS, 399, 497
- Fattahi, A., Navarro, J. F., Sawala, T., et al. 2016, MNRAS, 457, 844
- Gilman, D., Du, X., Benson, A., et al. 2019, MNRAS, L167
- Hsueh, J. W., Enzi, W., Vegetti, S., et al. 2019, MNRAS, 2780
- Komatsu, E., Smith, K. M., Dunkley, J., et al. 2011, ApJS, 192, 18
- Lovell, M. R. 2020, MNRAS, 493, L11
- Lovell, M. R., Frenk, C. S., Eke, V. R., et al. 2014, MNRAS, 439, 300
- Lovell, M. R., Bose, S., Boyarsky, A., et al. 2016, MNRAS, 461, 60
- . 2017, MNRAS, 468, 4285
- Lovell, M. R., Barnes, D., Bahé, Y., et al. 2019, MNRAS, 485, 4071
- Ludlow, A. D., Bose, S., Angulo, R. E., et al. 2016, MNRAS, 460, 1214
- Onions, J., Knebe, A., Pearce, F. R., et al. 2012, MNRAS, 423, 1200
- Oppenheimer, B. D., Crain, R. A., Schaye, J., et al. 2016, MNRAS, 460, 2157
- Planck Collaboration, Ade, P. A. R., Aghanim, N., et al. 2014, A&A, 571, A16
- Press, W. H., & Schechter, P. 1974, ApJ, 187, 425
- Sawala, T., Frenk, C. S., Fattahi, A., et al. 2016, MNRAS, 457, 1931
- Schaye, J., Crain, R. A., Bower, R. G., et al. 2015, MNRAS, 446, 521
- Schneider, A., Smith, R. E., Macciò, A. V., & Moore, B. 2012, MNRAS, 424, 684
- Springel, V., White, S. D. M., Tormen, G., & Kauffmann, G. 2001, MNRAS, 328, 726
- Viel, M., Lesgourgues, J., Haehnelt, M. G., Matarrese, S., & Riotto, A. 2005, PhRvD, 71, 063534
- Wang, J., & White, S. D. M. 2007, MNRAS, 380, 93